NASA
Technical
Paper
2455

July 1985

A Cracked Orthotropic Sheet Stiffened by a Semi-Infinite Orthotropic Sheet

C. A. Bigelow

NASA Technical Paper 2455

1985

A Cracked Orthotropic Sheet Stiffened by a Semi-Infinite Orthotropic Sheet

C. A. Bigelow

Langley Research Center
Hampton, Virginia

National Aeronautics and Space Administration

Scientific and Technical Information Branch

Summary

Although stringers are used primarily as stiffeners, they also can make damaged structures fail-safe or damage tolerant. Assessment of the damage tolerance of structures weakened by cracks is aided by knowledge of stress-intensity factors. In this paper, the stress-intensity factor is determined for a cracked orthotropic sheet adhesively bonded to an orthotropic stringer. Since the stringer is modeled as a semi-infinite sheet, the solution is most appropriate for a crack tip located near a stringer edge. Both adherends are treated as homogeneous, orthotropic media which are representative of many fiber-reinforced composite materials. It is assumed that the adherends are in a state of plane stress and the adhesive is in pure shear. By use of Green's functions and the complex variable theory of orthotropic elasticity developed by Lekhnitskii, a set of integral equations is obtained. The integral equations are replaced by an equivalent set of algebraic equations, which is solved to obtain the shear-stress distribution in the adhesive layer. From these adhesive stresses, equations for the stress-intensity factors at both crack tips are found.

A parametric study is also conducted to determine the sensitivity of the system to material properties and specimen configuration. The parameter having the greatest influence on the stress-intensity factors is the distance from the near crack tip to the edge of the stringer. Unless the crack tip is very close to or under the stringer, the stress-intensity factor is approximately that of an unstiffened sheet. However, as the crack propagates beneath the stringer, the stress-intensity factor decreases significantly. Increasing the stringer stiffness or the adhesive stiffness also results in a decrease in the stress-intensity factor.

Introduction

Because of their high strength and light weight, composite materials are finding increasing application in aerospace structures. In general, the structural configurations used in composite airplanes have been very similar to the sheet-stringer construction currently used in metal airplanes. In metal airplanes, stringers are effective in making damaged structures fail-safe or damage tolerant. For this reason, the interaction of a cracked sheet and a stringer is an important problem which has been investigated by many authors.

Romualdi, Frasier, and Irwin (ref. 1) considered two problems: a crack centrally located under a riveted stringer and a crack centrally located between two riveted stringers. In their formulation of the problem, only the two rivets nearest the crack were considered effective. Sanders (ref. 2) considered the problem of a crack positioned symmetrically beneath a continuously attached stringer. He employed a shear-lag line stringer and assumed the sheet to be inextensible in the direction parallel to the crack to obtain the stringer stress-concentration factor and the crack-tip stress-intensity factor. Greif and Sanders (ref. 3) removed Sanders' previous inextensionality assumption and symmetry requirements. They concluded that the stringer-induced reduction in the stress-intensity factor was a localized effect and that the stringer stress-concentration factor was largely insensitive to sheet stiffness in the direction parallel to the crack. Bloom and Sanders (ref. 4) reported an analysis of a discretely attached stringer which may be broken. Poe (ref. 5) examined the problem of a cracked sheet stiffened by evenly spaced, riveted longitudinal stringers. The crack was assumed to originate at a rivet location and to grow beneath intact stringers. An extension of that work (ref. 6) considered the influence of broken stringers.

Arin (ref. 7) examined the effect of the debonding of an infinitely long line stringer on the stress-intensity factor at the crack tip. He assumed that the stringer was adhesively bonded to an isotropic sheet along a line perpendicular to the crack. He concluded that the stringer exerts little influence on the stress-intensity factors unless it is quite close to the crack tip and the debond length is less than twice the crack length.

Norris (ref. 8), using a complex-variable approach, represented the finite-width stringer with an array of line stiffeners. The stringer was divided into strips, and each strip was represented by a line stiffener attached to the sheet at discrete points, with no coupling between adjacent line elements. Because the analysis did not model debonding of the adhesive, it predicted unrealistically high loads in the line stiffener nearest the crack tip.

Experimental work has shown that as the crack tip approaches the stringer, debonding can start and propagate through the adhesive. Although Arin (ref. 7) included adhesive debonding in his analysis, he modeled the stringer as a line, and thus was unable to account for partial debonding across the width of the stringer. Anderson, Hsu, and McGee (ref. 9) modeled partial debonding in their analysis of a cracked sheet reinforced by a bonded doubler. However, they were using a finite-element analysis, which would be very cumbersome and expensive to use when varying parameters such as crack length and debond area.

A realistic analysis is needed that examines the effect of growing debond area on crack propagation in adhesively bonded structures. The purpose of this

paper is to formulate such an analysis and to use it to study orthotropic sheets reinforced by orthotropic stringers. To meet this objective, the problem has been divided into two parts. In the first part, the problem is formulated with the assumption of a linear elastic adhesive with no debonding, and the stringer is modeled as a semi-infinite sheet bonded to an infinite sheet containing a crack. In the second part, the effects of adhesive nonlinearity and debonding are included. Although both parts have been solved, for brevity only the first part of the problem is presented here.

Nomenclature

a	half-length of crack, m
$+a$	right crack tip, m
$-a$	left crack tip, m
A_j, B_j, C_j, D_j	constant coefficients in layer j stress functions, N/m^3
b	distance from edge of stringer to center of crack, m
C_{jk}	complex constants $(j, k = 1, 2)$
D	domain of integration
E_x, E_y	Young's moduli in the x- and y-directions, respectively, Pa
$F_D(w, z, a)$	complex-variable function used in displacement-potential functions
$F_F(w, a)$	complex-variable function used in calculation of left crack-tip stress-intensity factor
$F_G(w, z, a)$	complex-variable function used in displacement functions of layer 2
$F_H(z, w, a)$	complex-variable function used in stress potentials
$F_I(w, a)$	complex-variable function used in calculation of right crack-tip stress-intensity factor
f_{01}, f_{02}	stress functions, m^3/N
G_{xy}	orthotropic shear modulus, Pa
G_3	shear modulus of adhesive layer, Pa
h_j	thickness of layer j, m
i	$= \sqrt{-1}$
k_1	normal (mode I) component of stress-intensity factor, $Pa\sqrt{m}$
N	number of collocation points; number of cells in the domain
p_j, q_j	complex constants for orthotropic sheet $(j = 1, 2)$, 1/Pa
Q_{jk}, R_{jk}	complex kernels used in displacement functions for layers 1 and 2, respectively $(j, k = 1, 2)$, 1/Pa
S_{jk}	complex kernels used in integral equations $(j, k = 1, 2)$, 1/(Pa-m)
T_j	complex kernels used in stress-intensity factors (j = 1, 2, 3, 4)
u_j, v_j	x- and y-displacements of layer j, m
$u_1^{(b)}, v_1^{(b)}$	displacements in layer 1 due to crack-face pressure, m
u^c, v^c	displacements in layer 1 due to concentrated forces, m
$u_1^{(c)}, v_1^{(c)}$	displacements in layer 1 due to distributed body forces, m
u^s, v^s	displacements in layer 2 due to a pair of concentrated forces, m
u_2', v_2'	displacements in layer 2 due to distributed body forces, with respect to rotated coordinate system, m
w_j	complex variable (j = 1, 2, 3, 4), m
X_j, Y_j	body forces acting on layer j (j = 1, 2), N/m^3
X_2', Y_2'	layer 2 body forces in rotated coordinate system, N/m^3
x, y	Cartesian coordinates, m
x_0, y_0	coordinates of load point, m
x', y'	rotated coordinate system, m
z_j	complex variable (j = 1, 2), m
z_0	location of load point, m
$\Delta x_n, \Delta y_n$	incremental distances $(n = 1, 2, \ldots, N)$, m

μ_j	roots of the characteristic equation ($j = 1, 2$)
ν_{xy}, ν_{yx}	Poisson's ratios
σ_0	pressure applied to crack face, Pa
τ_x, τ_y	shear stresses in adhesive layer, Pa
$\phi_1'(z), \phi_2'(z)$	stress potentials for orthotropic materials, Pa
$\phi_1^c(z), \phi_2^c(z)$	displacement potentials due to a pair of load points in the cracked sheet, m
$\phi_1^{(2)}(z), \phi_2^{(2)}(z)$	displacement potentials due to a pair of load points in a half-plane, m

Superscripts:

$(j), (k)$	layer number ($j, k = 1,2$)

A bar over a symbol indicates a complex conjugate; thus, if $z = x + iy$, then $\bar{z} = x - iy$. A prime on a symbol indicates reference to the rotated coordinate system, except in the stress and displacement potentials, for which a prime indicates differentiation.

Formulation of the Problem

Consider the sheet-stringer configuration shown in figure 1. (Hereinafter, the semi-infinite sheet will be referred to as a stringer.) The stringer and the sheet are bonded together by an adhesive layer of constant thickness h_3. Here the bond is assumed to be intact. The crack faces are subjected to a uniform pressure σ_0 and the stress state at infinity is zero, as shown in part A of figure 2. The problem is solved with the following assumptions:

1. The sheet (layer 1), the stringer (layer 2), and the adhesive (layer 3) are homogeneous and linearly elastic.
2. The sheet and the stringer are dissimilar, orthotropic materials with principal directions of orthotropy being oriented parallel and perpendicular to the crack in layer 1.
3. The thicknesses of the sheet and the stringer are small compared with the in-plane dimensions, so that both layers are considered to be in a state of plane stress.
4. The surface shear transmitted through the adhesive is assumed to act as a body force on the adherends.
5. The thickness of the adhesive is small compared with the thicknesses of the sheet and the stringer; thus, the adhesive layer is treated as a shear spring rather than as an elastic continuum.

Assumption 5 leads to the following continuity of displacement equations:

$$u_1 - u_2 = \frac{h_3}{G_3}\tau_x \qquad v_1 - v_2 = \frac{h_3}{G_3}\tau_y \tag{1}$$

where u_1, v_1 and u_2, v_2 are the x- and y-components of the in-plane displacement vectors in layers 1 and 2, τ_x and τ_y are the components of the adhesive shear stress, and h_3 and G_3 are the adhesive thickness and shear modulus, respectively. From assumption 3, the two sets of body forces (forces per unit volume) that act on layers 1 and 2 can be written as follows:

$$X_1 = -\frac{\tau_x}{h_1} \qquad Y_1 = -\frac{\tau_y}{h_1} \qquad X_2 = \frac{\tau_x}{h_2} \qquad Y_2 = \frac{\tau_y}{h_2} \tag{2}$$

Figure 2 shows how the problem is broken into its component parts. The displacements in the sheet, shown in part B of figure 2, and in the stringer, shown in part C of figure 2, are determined individually as follows.

Displacements in the Sheet (Layer 1)

The forces acting on the sheet (layer 1) are shown in figure 3. The cracked sheet is subjected to the body forces X_1 and Y_1 distributed over the domain D and to the crack-face pressure σ_0. The problem shown in part A of figure 3 is equivalent to the superposition of the problems shown in parts B and C of figure 3.

If $u_1^{(b)}, v_1^{(b)}$ and $u_1^{(c)}, v_1^{(c)}$ denote the displacements in the sheet due to the loadings shown in parts B and C, respectively, of figure 3, the total displacements in the sheet can be written as

$$u_1 = u_1^{(b)} + u_1^{(c)} \qquad v_1 = v_1^{(b)} + v_1^{(c)} \tag{3}$$

If we follow Lekhnitskii (ref. 10) and ignore an arbitrary rigid-body displacement vector, the displacements $u_1^{(b)}$ and $v_1^{(b)}$ due to the crack-face pressure σ_0, shown in part B of figure 3, can be found. The complete expressions for $u_1^{(b)}$ and $v_1^{(b)}$ are given in appendix A.

Determination of the displacements $u_1^{(c)}$ and $v_1^{(c)}$ due to the distributed body forces shown in part C of figure 3 starts with the known displacements due to a concentrated force located at the point $z_0 = x_0 + iy_0$. Since the body forces X_1 and Y_1 are continuous functions of z_0 in the domain D, the displacements due to the concentrated forces can be used as Green's functions to determine $u_1^{(c)}$ and $v_1^{(c)}$. Thus, these displacements can be written as follows:

$$\left.\begin{aligned} u_1^{(c)}(x,y) &= \iint_D \left[Q_{11}\left(x,y,x_0,y_0\right) X_1\left(x_0,y_0\right) + Q_{12}\left(x,y,x_0,y_0\right) Y_1\left(x_0,y_0\right)\right] dx_0\, dy_0 \\ v_1^{(c)}(x,y) &= \iint_D \left[Q_{21}\left(x,y,x_0,y_0\right) X_1\left(x_0,y_0\right) + Q_{22}\left(x,y,x_0,y_0\right) Y_1\left(x_0,y_0\right)\right] dx_0\, dy_0 \end{aligned}\right\} \tag{4}$$

where Q_{11}, Q_{12}, Q_{21}, and Q_{22} are derived in appendix A.

Displacements in the Stringer (Layer 2)

The only forces acting on the semi-infinite stringer (layer 2) are the distributed body forces X_2 and Y_2 shown in part C of figure 2. In a procedure similar to that used in reference 11, the displacements due to a single pair of body forces X_2' and Y_2', located at point $z_0' = x_0' + iy_0'$ (see fig. 4), are used to form the displacements u_2' and v_2' due to the distributed loading. Since the body forces X_2' and Y_2' are continuous functions of z_0' in the domain, the displacements due to the concentrated force can be used as Green's functions for the total displacements u_2' and v_2'. Thus, these displacements can be written as follows:

$$\left.\begin{aligned} u_2'(x',y') &= \iint_D \left[R_{11}\left(x',y',x_0',y_0'\right) X_2'\left(x_0',y_0'\right) + R_{12}\left(x',y',x_0',y_0'\right) Y_2'\left(x_0',y_0'\right)\right] dx_0'\, dy_0' \\ v_2'(x',y') &= \iint_D \left[R_{21}\left(x',y',x_0',y_0'\right) X_2'\left(x_0',y_0'\right) + R_{22}\left(x',y',x_0',y_0'\right) Y_2'\left(x_0',y_0'\right)\right] dx_0'\, dy_0' \end{aligned}\right\} \tag{5}$$

The expressions for R_{11}, R_{12}, R_{21}, and R_{22} are derived in appendix B.

The displacements u_2 and v_2, required for the loading shown in part C of figure 2, are calculated by shifting and rotating the displacements u_2' and v_2' according to the following relations:

$$u_2(x,y) = -v_2'(x',y') \qquad v_2(x,y) = u_2'(x',y') \tag{6}$$

where

$$x' = y \qquad y' = b - x$$
$$X_2' = Y_2 \qquad Y_2' = -X_2$$

Complete details on the derivation of the displacements for the stringer are presented in appendix B.

Integral Equations for τ_x and τ_y

Substituting equations (3) and (6) into equations (1) yields the following system of integral equations for the unknown functions τ_x and τ_y:

$$\left.\begin{aligned}
&\frac{h_3}{G_3}\tau_x(x,y) + \iint_D \left\{\left[\frac{Q_{11}}{h_1}(x,y,x_0,y_0) + \frac{R_{22}}{h_2}\left(x',y',x_0',y_0'\right)\right]\tau_x\left(x_0,y_0\right)\right. \\
&\qquad \left. + \left[\frac{Q_{12}}{h_1}\left(x,y,x_0,y_0\right) - \frac{R_{21}}{h_2}\left(x',y',x_0',y_0'\right)\right]\tau_y\left(x_0,y_0\right)\right\} dx_0\, dy_0 = \sigma_0 f_{01}(x,y) \\
&\frac{h_3}{G_3}\tau_y(x,y) + \iint_D \left\{\left[\frac{Q_{21}}{h_1}\left(x,y,x_0,y_0\right) - \frac{R_{12}}{h_2}\left(x',y',x_0',y_0'\right)\right]\tau_x\left(x_0,y_0\right)\right. \\
&\qquad \left. + \left[\frac{Q_{22}}{h_1}\left(x,y,x_0,y_0\right) + \frac{R_{11}}{h_2}\left(x',y',x_0',y_0'\right)\right]\tau_y\left(x_0,y_0\right)\right\} dx_0\, dy_0 = \sigma_0 f_{02}(x,y)
\end{aligned}\right\} \tag{7}$$

where

$$\left.\begin{aligned}
f_{01}(x,y) &= \text{Real}\left\{\frac{1}{\mu_1^{(1)} - \mu_2^{(1)}}\left[p_1^{(1)}\mu_2^{(1)}\left(z_1^{(1)} - \sqrt{z_1^{(1)^2} - a^2}\right)\right.\right. \\
&\qquad \left.\left. - p_2^{(1)}\mu_1^{(1)}\left(z_2^{(1)} - \sqrt{z_2^{(1)^2} - a^2}\right)\right]\right\} \\
f_{02}(x,y) &= \text{Real}\left\{\frac{1}{\mu_1^{(1)} - \mu_2^{(1)}}\left[q_1^{(1)}\mu_2^{(1)}\left(z_1^{(1)} - \sqrt{z_1^{(1)^2} - a^2}\right)\right.\right. \\
&\qquad \left.\left. - q_2^{(1)}\mu_1^{(1)}\left(z_2^{(1)} - \sqrt{z_2^{(1)^2} - a^2}\right)\right]\right\} \\
x_0' &= y_0 \\
y_0' &= b - x_0 \\
x' &= y \\
y' &= b - x
\end{aligned}\right\} \tag{8}$$

The parenthetical numerical superscripts indicate layer number.

As in reference 7, the kernels Q_{jk} and R_{jk} $(j,k = 1,2)$, which have logarithmic singularities, are known and are integrable in the domain D. Thus, equations (7) can be treated as Fredholm's integral equations of the second kind and can be solved numerically by reducing them to a system of linear algebraic equations. If the integral signs are replaced by summations and collocation is used, the following system of linear equations in the unknowns $\tau_x(x,y)$ and $\tau_y(x,y)$ is obtained:

$$\left.\begin{aligned}
&\frac{h_3}{G_3}\tau_x(x_j,y_j) + \sum_{n=1}^{N}\left[S_{11}\left(x_j,y_j,x_{0_n},y_{0_n}\right)\tau_x\left(x_{0_n},y_{0_n}\right)\right. \\
&\qquad \left. + S_{12}\left(x_j,y_j,x_{0_n},y_{0_n}\right)\tau_y\left(x_{0_n},y_{0_n}\right)\right]\Delta x_n \Delta y_n = \sigma_0 f_{01}\left(x_j,y_j\right) \qquad (j = 1,N) \\
&\frac{h_3}{G_3}\tau_y\left(x_j,y_j\right) + \sum_{n=1}^{N}\left[S_{21}\left(x_j,y_j,x_{0_n},y_{0_n}\right)\tau_x\left(x_{0_n},y_{0_n}\right)\right. \\
&\qquad \left. + S_{22}\left(x_j,y_j,x_{0_n},y_{0_n}\right)\tau_y\left(x_{0_n},y_{0_n}\right)\right]\Delta x_n \Delta y_n = \sigma_0 f_{02}\left(x_j,y_j\right) \qquad (j = 1,N)
\end{aligned}\right\} \tag{9}$$

where

$$S_{11} = \frac{Q_{11}}{h_1} + \frac{R_{22}}{h_2} \tag{10a}$$

$$S_{12} = \frac{Q_{12}}{h_1} - \frac{R_{21}}{h_2} \tag{10b}$$

$$S_{21} = \frac{Q_{21}}{h_1} - \frac{R_{12}}{h_2} \tag{10c}$$

$$S_{22} = \frac{Q_{22}}{h_1} + \frac{R_{11}}{h_2} \tag{10d}$$

and N is the number of collocation points. The terms Q_{jk} and R_{jk} $(j,k = 1,2)$ are defined in appendixes A and B, respectively.

The Stress-Intensity Factor

In the present problem, because of symmetries in geometry and loading, the shear component of the stress-intensity factor is zero. The normal component is found by combining the effects of the crack-face pressure and the distributed body forces $X_1(x,y)$ and $Y_1(x,y)$ acting on layer 1. The stress-intensity factor may be expressed in terms of the unknowns τ_x and τ_y as follows:

$$k_1(a_0) = \sigma_0\sqrt{a} + \frac{2a_0}{a\sqrt{a}h_1}\iint_D \left[T_1(x,y,x_0,y_0)\,\tau_x(x_0,y_0) + T_2(x,y,x_0,y_0)\,\tau_y(x_0,y_0)\right] dx_0\,dy_0 \tag{11}$$

where

$$T_1(x,y,x_0,y_0) = C_{11}^{(1)}\left[F_I\left(w_1^{(1)},a\right) + F_I\left(w_3^{(1)},a\right)\right] + C_{21}^{(1)}\left[F_I\left(w_2^{(1)},a\right) + F_I\left(w_4^{(1)},a\right)\right]$$

$$T_2(x,y,x_0,y_0) = C_{12}^{(1)}\left[F_I\left(w_1^{(1)},a\right) + F_I\left(w_3^{(1)},a\right)\right] + C_{22}^{(1)}\left[F_I\left(w_2^{(1)},a\right) + F_I\left(w_4^{(1)},a\right)\right]$$

$$F_I(w,a) = \frac{\sqrt{w^2-a^2} - (w-a_0)}{w-a_0}$$

and a_0 is replaced by $+a$ for the right crack tip and by $-a$ for the left crack tip. Complete details of the derivation of the equation for stress-intensity factors are given in appendix C.

The solution of equations (9) gives the shear-stress distribution in the adhesive layer $\tau_x(x,y)$ and $\tau_y(x,y)$. Using these adhesive shear stresses in equations (11), we can determine the stress-intensity factors at either crack tip. The numerical solution to the problem is discussed in the next section.

Numerical Solution

A key item in the analysis is the method of integration used for the system of integral equations represented by equations (7). In theory, these equations require integration over the infinite domain. However, because of the complicated nature of these equations, a closed-form integration is probably impossible. Consequently, the system of Fredholm's integral equations is solved with standard numerical techniques. This is done by dividing the domain into cells, assuming the unknown functions τ_x and τ_y to be uniform in each cell, and then using a numerical scheme to evaluate integrals. In this way the system of integral equations is reduced to the system of algebraic equations given by equations (9). Two important aspects of the numerical integration are the domain of integration and the logarithmic singularities in the kernels.

In order to carry out the numerical analysis, the size of the infinite domain must be restricted. This restriction is possible because the disturbance caused by the presence of the crack decays with distance from the crack. A convergence study has been conducted to ensure that restricting the domain does not appreciably affect the accuracy of the results. Thus, the size of the domain D is determined iteratively, starting with a small, coarse-mesh domain and increasing the domain extent and mesh refinement until no significant changes occur in the quantities of interest.

The second aspect of the integral equations requiring special attention concerns the kernels S_{jk} which appear in equations (9). These kernels contain logarithmic singularities which must be evaluated separately. This is done by performing an exact integration of the singular portion of the kernels over the segment Δx_n. In effect, this integration applies the load over a finite length rather than at a single point, thereby removing the singularity.

Discussion of Results

To gain insight into the behavior of the stringer panel, the analysis was performed for numerous combinations of material and geometric parameters.

Three different materials were assumed for the sheet. Their properties are given in table I. Material 4, also shown in table I, was used to model the stringer. These materials span a wide range of properties and are representative of frequently used graphite/epoxy laminates (ref. 12).

Figure 5 shows the normalized stress-intensity factor as a function of b/a, the ratio of the stringer edge distance to the crack half-length. Here, the crack half-length a is held constant and b is increased. In this and all subsequent figures, the stress-intensity factors have been normalized with $\sigma_0\sqrt{a}$, the stress-intensity factor for a cracked, infinite sheet with a uniform pressure σ_0 applied to the crack face. As shown in this figure, once the right crack tip is no longer beneath the stringer, the reduction in k_1 is minimal. Also, the effect of the stringer on the left crack tip is much less than that on the right crack tip. This is to be expected, since the left crack tip is farther from the edge of the stringer. For large values of b/a, both the right and the left crack-tip stress intensities approach 1.00 (the value when no stringer is present), again as expected. Changing the material properties of the sheet does not greatly affect the value of k_1, although the lower the longitudinal stiffness of the sheet material, the greater the reduction in the stress intensity due to the presence of the stringer.

Figure 6 presents data similar to those shown in figure 5, but in a slightly different manner. In this case, b is held constant while a is increased. The stress-intensity factor is not affected by the presence of the stringer until the crack tip is very close to the edge of the stringer, and no significant reduction in k_1 occurs until the right crack tip is beneath the stringer itself. As in the previous figure, the stress-intensity factor at the left crack tip is not significantly affected by the stringer, and changing the material of the sheet does not have a large effect on k_1.

In figures 7 and 8, the effects of varying the stiffnesses of the stringer and the adhesive are examined. In these figures, material 1 is used for the sheet and material 4 for the stringer; two ratios of b/a, 1.2 and 0.5, are used. In these figures, only results for the right crack tip are shown, since any effects on the left crack-tip stress-intensity factor are minimal.

The effect of varying the stringer stiffness $E_y^{(2)}h_2$ is illustrated in figure 7. The normalized stress-intensity factor for the right crack tip is plotted as a function of the ratio of the stringer stiffness to the sheet stiffness. This figure shows that as the stringer stiffness approaches zero, the normalized k_1 approaches 1.00, the solution for a cracked sheet with no stringer. As the stringer stiffness increases, the curves approach a lower bound on k_1. This indicates that past a certain point, no further reductions in k_1 can be obtained by increasing the stringer stiffness. The value of this lower bound on k_1 is a function of the adhesive stiffness and b/a. Changing the stringer stiffness has much less effect on the stress-intensity factor for the case of $b/a = 1.2$ than for $b/a = 0.5$.

The effect of varying the adhesive shear stiffness G_3/h_3 is illustrated in figure 8. The normalized stress-intensity factor is plotted as a function of the ratio of the adhesive shear stiffness to the shear stiffness of the sheet. As the adhesive shear stiffness approaches zero, the value of k_1 tends toward 1.00, as expected. As the adhesive shear stiffness increases, k_1 decreases. For $b/a = 1.2$ the decrease is small, since the effect of the stringer is negligible. However, for $b/a = 0.5$, the decrease in k_1 is substantial. Although these points lie off the scale shown in figure 8, for very large values of G_3 (on the order of 10^{10} MPa), the stress-intensity factor does not approach zero (as might be expected) but rather some nonzero minimum value. This lower bound is a function of the stringer stiffness and b/a. Figure 8 also shows that for values of $G_3h_1/G_{xy}^{(1)}h_3$ greater than about 4.0, increasing the adhesive shear stiffness has little effect on the stress-intensity factor.

Concluding Remarks

This report has presented the formulation of an analysis for a cracked orthotropic sheet reinforced with an adhesively bonded orthotropic semi-infinite sheet. This configuration was assumed to represent a bonded stringer panel when the crack is located close to the edge of the stringer. The adhesive bond was also assumed to be intact. A parametric study was conducted to determine the sensitivity of the system to material properties and specimen configuration. The parameter having the greatest influence on the stress-intensity factor was the distance from the near crack tip to the edge of the stringer. Unless the crack was very close to or under the stringer, the reduction in k_1 was minimal, and the farther the crack was under the stringer, the greater the reduction in k_1. Increasing the stiffness of the stringer or of the adhesive also resulted in a reduction in the stress-intensity factor.

NASA Langley Research Center
Hampton, VA 23665
April 11, 1985

Appendix A

Derivation of Displacement Functions for Infinite Cracked Orthotropic Sheet

This appendix presents the derivation of the displacement functions for the infinite cracked orthotropic sheet (layer 1). If we follow Lekhnitskii (ref. 10) and ignore an arbitrary rigid-body displacement vector, the displacements due to the crack-face pressure σ_0 (shown in part B of figure 3) can be written as follows:

$$\left.\begin{aligned} u_1^{(b)} &= \text{Real}\left\{\frac{\sigma_0}{\mu_1^{(1)}-\mu_2^{(1)}}\left[p_1^{(1)}\mu_2^{(1)}\left(z_1^{(1)}-\sqrt{z_1^{(1)^2}-a^2}\right)-p_2^{(1)}\mu_1^{(1)}\left(z_2^{(1)}-\sqrt{z_2^{(1)^2}-a^2}\right)\right]\right\} \\ v_1^{(b)} &= \text{Real}\left\{\frac{\sigma_0}{\mu_1^{(1)}-\mu_2^{(2)}}\left[q_1^{(1)}\mu_2^{(1)}\left(z_1^{(1)}-\sqrt{z_1^{(1)^2}-a^2}\right)-q_2^{(1)}\mu_1^{(1)}\left(z_2^{(1)}-\sqrt{z_2^{(1)^2}-a^2}\right)\right]\right\} \end{aligned}\right\} \tag{A1}$$

where

$$a = \text{crack half-length}$$

$$z_j^{(1)} = x + \mu_j^{(1)} y \qquad (j = 1, 2)$$

$$p_j^{(k)} = \frac{1}{E_x^{(k)}}\left(\mu_j^2 - \nu_{xy}^{(k)}\right) \qquad (j = 1, 2;\ (k) = \text{ Layer number})$$

$$q_j^{(k)} = \frac{1}{E_y^{(k)}}\left(\frac{1}{\mu_j^{(k)}} - \nu_{yx}^{(k)}\mu_j^{(k)}\right) \qquad (j = 1, 2;\ (k) = \text{Layer number})$$

The terms $\mu_1^{(k)}$, $\mu_2^{(k)}$, $\bar{\mu}_1^{(k)}$, $\bar{\mu}_2^{(k)}$ are the roots of the characteristic equation

$$\mu^{(k)^4} + \left(\frac{E_x^{(k)}}{G_{xy}^{(k)}} - 2\nu_{xy}^{(k)}\right)\mu^{(k)^2} + \frac{E_x^{(k)}}{E_y^{(k)}} = 0 \qquad \left(\text{Im}\left(\mu_j^{(k)}\right) > 0\right)$$

where E_x and E_y are the Young's moduli, G_{xy} is the shear modulus, and ν_{xy} and ν_{yx} are the Poisson's ratios of the orthotropic sheet.

To determine the displacements for the distributed loading shown in part C of figure 3, start with the displacements for a concentrated force located at the point $z_0 = x_0 + iy_0$. The displacements for a concentrated force can be written as

$$\left.\begin{aligned} u^c(x,y) &= 2\ \text{Real}\left[p_1^{(1)}\phi_1^c\left(z_1^{(1)}\right) + p_2^{(2)}\phi_2^c\left(z_2^{(1)}\right)\right] \\ v^c(x,y) &= 2\ \text{Real}\left[q_1^{(1)}\phi_1^c\left(z_1^{(1)}\right) + q_2^{(1)}\phi_2^c\left(z_2^{(1)}\right)\right] \end{aligned}\right\} \tag{A2}$$

where

$$\begin{aligned} \phi_1^c\left(z_1^{(1)}\right) = &\frac{\mu_2^{(1)}}{\mu_1^{(1)}-\mu_2^{(1)}}\left[A_1 F_D\left(w_1^{(1)}, z_1^{(1)}, a\right) + B_1 F_D\left(w_2^{(1)}, z_1^{(1)}, a\right)\right. \\ &\left. + C_1 F_D\left(w_3^{(1)}, z_1^{(1)}, a\right) + D_1 F_D\left(w_4^{(1)}, z_1^{(1)}, a\right)\right] \\ &+ A_1 \log\left(z_1^{(1)} - w_1^{(1)}\right) + C_1 \log\left(z_1^{(1)} - w_3^{(1)}\right) \end{aligned}$$

$$\begin{aligned} \phi_2^c\left(z_2^{(1)}\right) = &\frac{-\mu_1^{(1)}}{\mu_1^{(1)}-\mu_2^{(1)}}\left[A_1 F_D\left(w_1^{(1)}, z_2^{(1)}, a\right) + B_1 F_D\left(w_2^{(1)}, z_2^{(1)}, a\right)\right. \\ &\left. + C_1 F_D\left(w_3^{(1)}, z_2^{(1)}, a\right) + D_1 F_D\left(w_4^{(1)}, z_2^{(1)}, a\right)\right] \\ &+ B_1 \log\left(z_2^{(1)} - w_2^{(1)}\right) + D_1 \log\left(z_2^{(1)} - w_4^{(1)}\right) \end{aligned}$$

$$F_D(w,z,a) = \log\left(\sqrt{w^2-a^2}\sqrt{z^2-a^2} + wz - a^2\right) - \log\left(\sqrt{z^2-a^2} + z\right)$$

$$\left.\begin{aligned} w_1^{(1)} &= x_0 + \mu_1^{(1)} y_0 & w_2^{(1)} &= x_0 + \mu_2^{(1)} y_0 \\ w_3^{(1)} &= x_0 - \mu_1^{(1)} y_0 & w_4^{(1)} &= x_0 - \mu_2^{(1)} y_0 \\ A_1 &= C_{11}^{(1)} X_1 + C_{12}^{(1)} Y_1 & B_1 &= C_{21}^{(1)} X_1 + C_{22}^{(1)} Y_1 \\ C_1 &= C_{11}^{(1)} X_1 - C_{12}^{(1)} Y_1 & D_1 &= C_{21}^{(1)} X_1 - C_{22}^{(1)} Y_1 \end{aligned}\right\} \tag{A3}$$

$$\left.\begin{aligned} C_{11}^{(j)} &= \frac{\mu_1^{(j)}\left[\bar{\mu}_1^{(j)}\left(1+\nu_{yx}^{(j)}\mu_2^{(j)}\bar{\mu}_2^{(j)}\right) + \bar{\mu}_2^{(j)} + \mu_2^{(j)}\right]}{2\pi i\left(\mu_1^{(j)} - \mu_2^{(j)}\right)\left(\mu_1^{(j)} - \bar{\mu}_1^{(j)}\right)\left(\mu_1^{(j)} - \bar{\mu}_2^{(j)}\right)} \\ C_{12}^{(j)} &= \frac{\mu_1^{(j)}\left[\left(\mu_2^{(j)} + \bar{\mu}_2^{(j)}\right)\bar{\mu}_1^{(j)} + \mu_2^{(j)}\bar{\mu}_2^{(j)} + \nu_{xy}^{(j)}\right]}{2\pi i\left(\mu_1^{(j)} - \mu_2^{(j)}\right)\left(\mu_1^{(j)} - \bar{\mu}_1^{(j)}\right)\left(\mu_1^{(j)} - \bar{\mu}_2^{(j)}\right)} \\ C_{21}^{(j)} &= \frac{\mu_2^{(j)}\left[\bar{\mu}_2^{(j)}\left(1+\nu_{yx}^{(j)}\mu_1^{(j)}\bar{\mu}_1^{(j)}\right) + \bar{\mu}_1^{(j)} + \mu_1^{(j)}\right]}{2\pi i\left(\mu_2^{(j)} - \mu_1^{(j)}\right)\left(\mu_2^{(j)} - \bar{\mu}_2^{(j)}\right)\left(\mu_2^{(j)} - \bar{\mu}_1^{(j)}\right)} \\ C_{22}^{(j)} &= \frac{\mu_2^{(j)}\left[\left(\bar{\mu}_1^{(j)} + \mu_1^{(j)}\right)\bar{\mu}_2^{(j)} + \mu_1^{(j)}\bar{\mu}_1^{(j)} + \nu_{xy}^{(j)}\right]}{2\pi i\left(\mu_2^{(j)} - \mu_1^{(j)}\right)\left(\mu_2^{(j)} - \bar{\mu}_2^{(j)}\right)\left(\mu_2^{(j)} - \bar{\mu}_1^{(j)}\right)} \end{aligned}\right\} \tag{A4}$$

Details on the derivation of $\phi_1^c\left(z_1^{(1)}\right)$ and $\phi_2^c\left(z_2^{(1)}\right)$ can be found in reference 13.

Since the body forces X_1 and Y_1 are continuous functions of z_0 in the domain D, the displacements u^c and v^c may be used as Green's functions to determine $u_1^{(c)}$ and $v_1^{(c)}$. The displacements $u_1^{(c)}$ and $v_1^{(c)}$ due to the body forces X_1 and Y_1 distributed over the domain can be written as follows:

$$\left.\begin{aligned} u_1^{(c)}(x,y) &= \iint_D u^c(x,y,x_0,y_0)\, dx_0\, dy_0 \\ &= \iint_D \left[Q_{11}(x,y,x_0,y_0) X_1(x_0,y_0) + Q_{12}(x,y,x_0,y_0) Y_1(x_0,y_0)\right] dx_0\, dy_0 \\ v_1^{(c)}(x,y) &= \iint_D v^c(x,y,x_0,y_0)\, dx_0\, dy_0 \\ &= \iint_D \left[Q_{21}(x,y,x_0,y_0) X_1(x_0,y_0) + Q_{22}(x,y,x_0,y_0) Y_1(x_0,y_0)\right] dx_0\, dy_0 \end{aligned}\right\} \tag{A5}$$

where Q_{11}, Q_{12}, Q_{21}, and Q_{22} are found by substituting equations (A2) into equations (A5) and then combining terms and simplifying. These expressions are shown below.

$$
\begin{aligned}
Q_{11}(x,y,x_0,y_0) = 2\ \mathrm{Real}\Bigg\{ & \frac{p_1^{(1)}\mu_2^{(1)}}{\mu_1^{(1)}-\mu_2^{(1)}}\left[C_{11}^{(1)}F_G\left(w_1^{(1)},z_1^{(1)},a\right)+C_{21}^{(1)}F_G\left(w_2^{(1)},z_1^{(1)},a\right)\right. \\
& \left. + C_{11}^{(1)}F_G\left(w_3^{(1)},z_1^{(1)},a\right)+C_{21}^{(1)}F_G\left(w_4^{(1)},z_1^{(1)},a\right)\right] \\
& - \frac{p_2^{(1)}\mu_1^{(1)}}{\mu_1^{(1)}-\mu_2^{(1)}}\left[C_{11}^{(1)}F_G\left(w_1^{(1)},z_2^{(1)},a\right)+C_{21}^{(1)}F_G\left(w_2^{(1)},z_2^{(1)},a\right)\right. \\
& \left. + C_{11}^{(1)}F_G\left(w_3^{(1)},z_2^{(1)},a\right)+C_{21}^{(1)}F_G\left(w_4^{(1)},z_2^{(1)},a\right)\right] \\
& - \frac{2\mu_2^{(1)}p_1^{(1)}\left(C_{11}^{(1)}+C_{21}^{(1)}\right)}{\mu_1^{(1)}-\mu_2^{(1)}}\left[\log\left(\sqrt{z_1^{(1)^2}-a^2}+z_1^{(1)}\right)\right] \\
& + \frac{2\mu_1^{(1)}p_2^{(1)}\left(C_{11}^{(1)}+C_{21}^{(1)}\right)}{\mu_1^{(1)}-\mu_2^{(1)}}\left[\log\left(\sqrt{z_2^{(1)^2}-a^2}+z_2^{(1)}\right)\right] \\
& + p_1^{(1)}C_{11}^{(1)}\left[\log\left(z_1^{(1)}-w_1^{(1)}\right)+\log\left(z_1^{(1)}-w_3^{(1)}\right)\right] \\
& \left. + p_2^{(1)}C_{21}^{(1)}\left[\log\left(z_2^{(1)}-w_2^{(1)}\right)+\log\left(z_2^{(1)}-w_4^{(1)}\right)\right]\right\}
\end{aligned}
$$

$$
\begin{aligned}
Q_{12}(x,y,x_0,y_0) = 2\ \mathrm{Real}\Bigg\{ & \frac{p_1^{(1)}\mu_2^{(1)}}{\mu_1^{(1)}-\mu_2^{(1)}}\left[C_{12}^{(1)}F_G\left(w_1^{(1)},z_1^{(1)},a\right)+C_{22}^{(1)}F_G\left(w_2^{(1)},z_1^{(1)},a\right)\right. \\
& \left. - C_{12}^{(1)}F_G\left(w_3^{(1)},z_1^{(1)},a\right)-C_{22}^{(1)}F_G\left(w_4^{(1)},z_1^{(1)},a\right)\right] \\
& - \frac{p_2^{(1)}\mu_1^{(1)}}{\mu_1^{(1)}-\mu_2^{(1)}}\left[C_{12}^{(1)}F_G\left(w_1^{(1)},z_2^{(1)},a\right)+C_{22}^{(1)}F_G\left(w_2^{(1)},z_2^{(1)},a\right)\right. \\
& \left. - C_{12}^{(1)}F_G\left(w_3^{(1)},z_2^{(1)},a\right)-C_{22}^{(1)}F_G\left(w_4^{(1)},z_2^{(1)},a\right)\right] \\
& + p_1^{(1)}C_{12}^{(1)}\left[\log\left(z_1^{(1)}-w_1^{(1)}\right)-\log\left(z_1^{(1)}-w_3^{(1)}\right)\right] \\
& \left. + p_2^{(1)}C_{22}^{(1)}\left[\log\left(z_2^{(1)}-w_2^{(1)}\right)-\log\left(z_2^{(1)}-w_4^{(1)}\right)\right]\right\}
\end{aligned}
$$

$$
\begin{aligned}
Q_{21}(x,y,x_0,y_0) = 2\ \mathrm{Real}\Bigg\{ & \frac{q_1^{(1)}\mu_2^{(1)}}{\mu_1^{(1)}-\mu_2^{(1)}}\left[C_{11}^{(1)}F_G\left(w_1^{(1)},z_1^{(1)},a\right)+C_{21}^{(1)}F_G\left(w_2^{(1)},z_1^{(1)},a\right)\right. \\
& \left. + C_{11}^{(1)}F_G\left(w_3^{(1)},z_1^{(1)},a\right)+C_{21}^{(1)}F_G\left(w_4^{(1)},z_1^{(1)},a\right)\right] \\
& - \frac{q_2^{(1)}\mu_1^{(1)}}{\mu_1^{(1)}-\mu_2^{(1)}}\left[C_{11}^{(1)}F_G\left(w_1^{(1)},z_2^{(1)},a\right)+C_{21}^{(1)}F_G\left(w_2^{(1)},z_2^{(1)},a\right)\right. \\
& \left. + C_{11}^{(1)}F_G\left(w_3^{(1)},z_2^{(1)},a\right)+C_{21}^{(1)}F_G\left(w_4^{(1)},z_2^{(1)},a\right)\right] \\
& - \frac{2\mu_2^{(1)}q_1^{(1)}\left(C_{11}^{(1)}+C_{21}^{(1)}\right)}{\mu_1^{(1)}-\mu_2^{(1)}}\left[\log\left(\sqrt{z_1^{(1)^2}-a^2}+z_1^{(1)}\right)\right]
\end{aligned}
$$

(Equation continued on next page.)

$$
\begin{aligned}
&+\frac{2\mu_1^{(1)}q_2^{(1)}\left(C_{11}^{(1)}+C_{21}^{(1)}\right)}{\mu_1^{(1)}-\mu_2^{(1)}}\left[\log\left(\sqrt{z_2^{(1)^2}-a^2}+z_2^{(1)}\right)\right]\\
&+q_1^{(1)}C_{11}^{(1)}\left[\log\left(z_1^{(1)}-w_1^{(1)}\right)+\log\left(z_1^{(1)}-w_3^{(1)}\right)\right]\\
&+q_2^{(1)}C_{21}^{(1)}\left[\log\left(z_2^{(1)}-w_2^{(1)}\right)+\log\left(z_2^{(1)}-w_4^{(1)}\right)\right]\Bigg\}
\end{aligned}
$$

$$
\begin{aligned}
Q_{22}\left(x,y,x_0,y_0\right)=2\ \mathrm{Real}\Bigg\{&\frac{q_1^{(1)}\mu_2^{(1)}}{\mu_1^{(1)}-\mu_2^{(1)}}\left[C_{12}^{(1)}F_G\left(w_1^{(1)},z_1^{(1)},a\right)+C_{22}^{(1)}F_G\left(w_2^{(1)},z_1^{(1)},a\right)\right.\\
&\left.-C_{12}^{(1)}F_G\left(w_3^{(1)},z_1^{(1)},a\right)-C_{22}^{(1)}F_G\left(w_4^{(1)},z_1^{(1)},a\right)\right]\\
&-\frac{q_2^{(1)}\mu_1^{(1)}}{\mu_1^{(1)}-\mu_2^{(1)}}\left[C_{12}^{(1)}F_G\left(w_1^{(1)},z_2^{(1)},a\right)+C_{22}^{(1)}F_G\left(w_2^{(1)},z_2^{(1)},a\right)\right.\\
&\left.-C_{12}^{(1)}F_G\left(w_3^{(1)},z_2^{(1)},a\right)-C_{22}^{(1)}F_G\left(w_4^{(1)},z_2^{(1)},a\right)\right]\\
&+q_1^{(1)}C_{12}^{(1)}\left[\log\left(z_1^{(1)}-w_1^{(1)}\right)-\log\left(z_1^{(1)}-w_3^{(1)}\right)\right]\\
&+q_2^{(1)}C_{22}^{(1)}\left[\log\left(z_2^{(1)}-w_2^{(1)}\right)-\log\left(z_2^{(1)}-w_4^{(1)}\right)\right]\Bigg\}
\end{aligned}
$$

where

$$
F_G(w,z,a)=\log\left(\sqrt{w^2-a^2}\sqrt{z^2-a^2}+wz-a^2\right)
$$

Appendix B

Derivation of Displacement Functions for Semi-Infinite Orthotropic Sheet

This appendix presents the derivation of the displacement functions for the semi-infinite orthotropic sheet (layer 2). The only forces acting on the semi-infinite sheet are the distributed body forces X_2 and Y_2, as shown in part C of figure 2. In a procedure similar to that used in reference 11, displacements due to a pair of body forces X_2' and Y_2', located at point $z_0' = x_0' + iy_0'$ and oriented as shown in figure 4, can be written as follows:

$$\left.\begin{aligned} u^s\left(x', y', x_0', y_0'\right) &= 2\,\mathrm{Real}\left[p_1^{(2)}\phi_1^{(2)}\left(z_1^{(2)}\right) + p_2^{(2)}\phi_2^{(2)}\left(z_2^{(2)}\right)\right] \\ v^s\left(x', y', x_0', y_0'\right) &= 2\,\mathrm{Real}\left[q_1^{(2)}\phi_1^{(2)}\left(z_1^{(2)}\right) + q_2^{(2)}\phi_2^{(2)}\left(z_2^{(2)}\right)\right] \end{aligned}\right\} \tag{B1}$$

where

$$\left.\begin{aligned} \phi_1^{(2)}\left(z_1^{(2)}\right) &= A_2 \log\left(z_1^{(2)} - w_1^{(2)}\right) + C_2 \log\left(z_1^{(2)} - w_3^{(2)}\right) \\ &\quad + \frac{1}{\mu_2^{(2)} - \mu_1^{(2)}}\left\{\left(\bar{\mu}_1^{(2)} - \mu_2^{(2)}\right)\left[\bar{A}_2 \log\left(z_1^{(2)} - \bar{w}_1^{(2)}\right)\right.\right. \\ &\quad \left. + \bar{C}_2 \log\left(z_1^{(2)} - \bar{w}_3^{(2)}\right)\right] + \left(\bar{\mu}_2^{(2)} - \mu_2^{(2)}\right) \\ &\quad \left.\times\left[\bar{B}_2 \log\left(z_1^{(2)} - \bar{w}_2^{(2)}\right) + \bar{D}_2 \log\left(z_1^{(2)} - \bar{w}_4^{(2)}\right)\right]\right\} \\ \phi_2^{(2)}\left(z_2^{(2)}\right) &= B_2 \log\left(z_2^{(2)} - w_2^{(2)}\right) + D_2 \log\left(z_2^{(2)} - w_4^{(2)}\right) \\ &\quad + \frac{1}{\mu_1^{(2)} - \mu_2^{(2)}}\left\{\left(\bar{\mu}_1^{(2)} - \mu_1^{(2)}\right)\left[\bar{A}_2 \log\left(z_2^{(2)} - \bar{w}_1^{(2)}\right)\right.\right. \\ &\quad \left. + \bar{C}_2 \log\left(z_2^{(2)} - \bar{w}_3^{(2)}\right)\right] + \left(\bar{\mu}_2^{(2)} - \mu_1^{(2)}\right) \\ &\quad \left.\times\left[\bar{B}_2 \log\left(z_2^{(2)} - \bar{w}_2^{(2)}\right) + \bar{D}_2 \log\left(z_2^{(2)} - \bar{w}_4^{(2)}\right)\right]\right\} \end{aligned}\right\} \tag{B2}$$

where

$$z_j^{(2)} = x_0' + \mu_j^{(2)} y_0' \qquad (j = 1, 2)$$

$$\begin{aligned} w_1^{(2)} &= x_0' + \mu_1^{(2)} y_0' & w_2^{(2)} &= x_0' + \mu_2^{(2)} y_0' \\ w_3^{(2)} &= -x_0' + \mu_1^{(2)} y_0' & w_4^{(2)} &= -x_0' + \mu_2^{(2)} y_0' \\ A_2 &= C_{11}^{(2)} X_2' + C_{12}^{(2)} Y_2' & B_2 &= C_{21}^{(2)} X_2' + C_{22}^{(2)} Y_2' \\ C_2 &= -C_{11}^{(2)} X_2' + C_{12}^{(2)} Y_2' & D_2 &= -C_{21}^{(2)} X_2' + C_{22}^{(2)} Y_2' \end{aligned}$$

and $C_{11}^{(2)}$, $C_{12}^{(2)}$, $C_{21}^{(2)}$, and $C_{22}^{(2)}$ are defined in equations (A4). Details on the derivation of $\phi_1^{(2)}\left(z_1^{(2)}\right)$ and $\phi_2^{(2)}\left(z_2^{(2)}\right)$ can be found in reference 13.

As before, if the body forces X_2' and Y_2' are continuous functions of z_0' in the domain, the displacements u^s and v^s, given by equations (B1), may be used as Green's functions for the displacements u_2' and v_2' due to the distributed forces. Thus, the displacements can be found as follows:

$$
\left.
\begin{aligned}
u_2'(x',y') &= \iint_D u^s(x',y',x_0',y_0')\, dx_0'\, dy_0' \\
&= \iint_D \left[R_{11}(x',y',x_0',y_0')\, X_2'(x_0',y_0') + R_{12}(x',y',x_0',y_0')\, Y_2'(x_0',y_0')\right] dx_0'\, dy_0' \\
v_2'(x',y') &= \iint_D v^s(x',y',x_0',y_0')\, dx_0'\, dy_0' \\
&= \iint_D \left[R_{21}(x',y',x_0',y_0')\, X_2'(x_0',y_0') + R_{22}(x',y',x_0',y_0')\, Y_2'(x_0',y_0')\right] dx_0'\, dy_0'
\end{aligned}
\right\} \tag{B3}
$$

where R_{11}, R_{12}, R_{21}, and R_{22} are found by substituting equations (B1) and (B2) into equations (B3) and then combining terms. The complete expressions for R_{11}, R_{12}, R_{21}, and R_{22} are given below.

Equations (B3) give the displacements of the semi-infinite sheet for the loading and the coordinate system shown in figure B1(a). However, the displacements u_2 and v_2 required for the solution are defined with respect to the coordinate system and are due to the forces X_2 and Y_2 shown in figure B1(b). Thus, from figure B1,

$$
u_2(x,y) = -v_2'(x',y') \qquad v_2(x,y) = u_2'(x',y') \tag{B4}
$$

where

$$
\begin{aligned}
x' &= y & y' &= b - x \\
X_2' &= Y_2 & Y_2' &= -X_2
\end{aligned}
$$

The displacements in the semi-infinite sheet (layer 2) are now found by combining equations (B1) and (B3) and substituting into equations (B4). Note that the material properties of layer 2 are defined with respect to the x', y' coordinate system (fig. 4).

Shown below are the complete expressions for the functions R_{11}, R_{12}, R_{21}, and R_{22}, which appear in equations (B3). Further details on the formulation of these expressions can be found in reference 13.

$$
\begin{aligned}
R_{11}(x',y',x_0',y_0') = 2\,\mathrm{Real}\Bigg(& p_1^{(2)} C_{11}^{(2)} \left[\log\left(z_1^{(2)} - w_1^{(2)}\right) - \log\left(z_1^{(2)} - w_3^{(2)}\right)\right] \\
& + p_2^{(2)} C_{21}^{(2)} \left[\log\left(z_2^{(2)} - w_2^{(2)}\right) - \log\left(z_2^{(2)} - w_4^{(2)}\right)\right] \\
& + \frac{p_1^{(2)}}{\mu_2^{(2)} - \mu_1^{(2)}} \Bigg\{ \left(\bar{\mu}_1^{(2)} - \mu_2^{(2)}\right) \bar{C}_{11}^{(2)} \left[\log\left(z_1^{(2)} - \bar{w}_1^{(2)}\right) - \log\left(z_1^{(2)} - \bar{w}_3^{(2)}\right)\right] \\
& + \left(\bar{\mu}_2^{(2)} - \mu_2^{(2)}\right) \bar{C}_{21}^{(2)} \left[\log\left(z_1^{(2)} - \bar{w}_2^{(2)}\right) - \log\left(z_1^{(2)} - \bar{w}_4^{(2)}\right)\right] \Bigg\} \\
& + \frac{p_2^{(2)}}{\mu_1^{(2)} - \mu_2^{(2)}} \Bigg\{ \left(\bar{\mu}_1^{(2)} - \mu_1^{(2)}\right) \bar{C}_{11}^{(2)} \left[\log\left(z_2^{(2)} - \bar{w}_1^{(2)}\right) - \log\left(z_2^{(2)} - \bar{w}_3^{(2)}\right)\right] \\
& + \left(\bar{\mu}_2^{(2)} - \mu_1^{(2)}\right) \bar{C}_{21}^{(2)} \left[\log\left(z_2^{(2)} - \bar{w}_2^{(2)}\right) - \log\left(z_2^{(2)} - \bar{w}_4^{(2)}\right)\right] \Bigg\} \Bigg)
\end{aligned}
$$

$$
\begin{aligned}
R_{12}\left(x', y', x_0', y_0'\right) = 2\,\mathrm{Real}\Big(& p_1^{(2)} C_{12}^{(2)} \left[\log\left(z_1^{(2)} - w_1^{(2)}\right) + \log\left(z_1^{(2)} - w_3^{(2)}\right)\right] \\
&+ p_2^{(2)} C_{22}^{(2)} \left[\log\left(z_2^{(2)} - w_2^{(2)}\right) + \log\left(z_2^{(2)} - w_4^{(2)}\right)\right] \\
&+ \frac{p_1^{(2)}}{\mu_2^{(2)} - \mu_1^{(2)}} \left\{\left(\bar{\mu}_1^{(2)} - \mu_2^{(2)}\right) \bar{C}_{12}^{(2)} \left[\log\left(z_1^{(2)} - \bar{w}_1^{(2)}\right) + \log\left(z_1^{(2)} - \bar{w}_3^{(2)}\right)\right]\right. \\
&\left. + \left(\bar{\mu}_2^{(2)} - \mu_2^{(2)}\right) \bar{C}_{22}^{(2)} \left[\log\left(z_1^{(2)} - \bar{w}_2^{(2)}\right) + \log\left(z_1^{(2)} - \bar{w}_4^{(2)}\right)\right]\right\} \\
&+ \frac{p_2^{(2)}}{\mu_1^{(2)} - \mu_2^{(2)}} \left\{\left(\bar{\mu}_1^{(2)} - \mu_1^{(2)}\right) \bar{C}_{12}^{(2)} \left[\log\left(z_2^{(2)} - \bar{w}_1^{(2)}\right) + \log\left(z_2^{(2)} - \bar{w}_3^{(2)}\right)\right]\right. \\
&\left. + \left(\bar{\mu}_2^{(2)} - \mu_1^{(2)}\right) \bar{C}_{22}^{(2)} \left[\log\left(z_2^{(2)} - \bar{w}_2^{(2)}\right) + \log\left(z_2^{(2)} - \bar{w}_4^{(2)}\right)\right]\right\}\Big)
\end{aligned}
$$

$$
\begin{aligned}
R_{21}\left(x', y', x_0', y_0'\right) = 2\,\mathrm{Real}\Big(& q_1^{(2)} C_{11}^{(2)} \left[\log\left(z_1^{(2)} - w_1^{(2)}\right) - \log\left(z_1^{(2)} - w_3^{(2)}\right)\right] \\
&+ q_2^{(2)} C_{21}^{(2)} \left[\log\left(z_2^{(2)} - w_2^{(2)}\right) - \log\left(z_2^{(2)} - w_4^{(2)}\right)\right] \\
&+ \frac{q_1^{(2)}}{\mu_2^{(2)} - \mu_1^{(2)}} \left\{\left(\bar{\mu}_1^{(2)} - \mu_2^{(2)}\right) \bar{C}_{11}^{(2)} \left[\log\left(z_1^{(2)} - \bar{w}_1^{(2)}\right) - \log\left(z_1^{(2)} - \bar{w}_3^{(2)}\right)\right]\right. \\
&\left. + \left(\bar{\mu}_2^{(2)} - \mu_2^{(2)}\right) \bar{C}_{21}^{(2)} \left[\log\left(z_1^{(2)} - \bar{w}_2^{(2)}\right) - \log\left(z_1^{(2)} - \bar{w}_4^{(2)}\right)\right]\right\} \\
&+ \frac{q_2^{(2)}}{\mu_1^{(2)} - \mu_2^{(2)}} \left\{\left(\bar{\mu}_1^{(2)} - \mu_1^{(2)}\right) \bar{C}_{11}^{(2)} \left[\log\left(z_2^{(2)} - \bar{w}_1^{(2)}\right) - \log\left(z_2^{(2)} - \bar{w}_3^{(2)}\right)\right]\right. \\
&\left. + \left(\bar{\mu}_2^{(2)} - \mu_1^{(2)}\right) \bar{C}_{21}^{(2)} \left[\log\left(z_2^{(2)} - \bar{w}_2^{(2)}\right) - \log\left(z_2^{(2)} - \bar{w}_4^{(2)}\right)\right]\right\}\Big)
\end{aligned}
$$

$$
\begin{aligned}
R_{22}\left(x', y', x_0', y_0'\right) = 2\,\mathrm{Real}\Big(& q_1^{(2)} C_{12}^{(2)} \left[\log\left(z_1^{(2)} - w_1^{(2)}\right) + \log\left(z_1^{(2)} - w_3^{(2)}\right)\right] \\
&+ q_2^{(2)} C_{22}^{(2)} \left[\log\left(z_2^{(2)} - w_2^{(2)}\right) + \log\left(z_2^{(2)} - w_4^{(2)}\right)\right] \\
&+ \frac{q_1^{(2)}}{\mu_2^{(2)} - \mu_1^{(2)}} \left\{\left(\bar{\mu}_1^{(2)} - \mu_2^{(2)}\right) \bar{C}_{12}^{(2)} \left[\log\left(z_1^{(2)} - \bar{w}_1^{(2)}\right) + \log\left(z_1^{(2)} - \bar{w}_3^{(2)}\right)\right]\right. \\
&\left. + \left(\bar{\mu}_2^{(2)} - \mu_2^{(2)}\right) \bar{C}_{22}^{(2)} \left[\log\left(z_1^{(2)} - \bar{w}_2^{(2)}\right) + \log\left(z_1^{(2)} - \bar{w}_4^{(2)}\right)\right]\right\} \\
&+ \frac{q_2^{(2)}}{\mu_1^{(2)} - \mu_2^{(2)}} \left\{\left(\bar{\mu}_1^{(2)} - \mu_1^{(2)}\right) \bar{C}_{12}^{(2)} \left[\log\left(z_2^{(2)} - \bar{w}_1^{(2)}\right) + \log\left(z_2^{(2)} - \bar{w}_3^{(2)}\right)\right]\right. \\
&\left. + \left(\bar{\mu}_2^{(2)} - \mu_1^{(2)}\right) \bar{C}_{22}^{(2)} \left[\log\left(z_2^{(2)} - \bar{w}_2^{(2)}\right) + \log\left(z_2^{(2)} - \bar{w}_4^{(2)}\right)\right]\right\}\Big)
\end{aligned}
$$

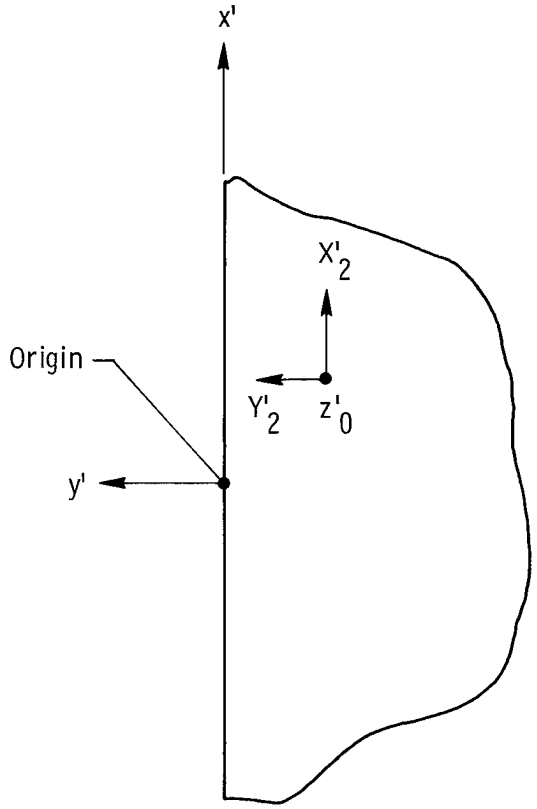

(a) System definition used in solution.

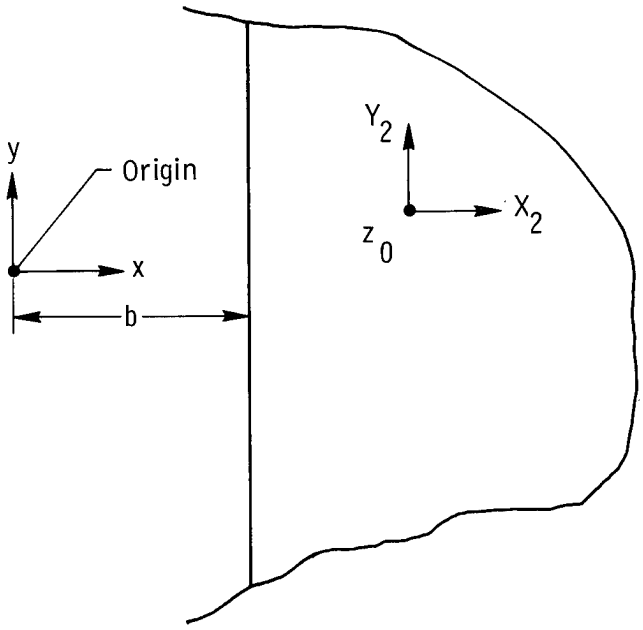

(b) System definition used in integral equations.

Figure B1. Shift and rotation of coordinate system for half-plane solution.

Appendix C

Derivation of Stress-Intensity Factor Equations

This appendix presents the derivation of the stress-intensity factor equations. In the present problem, because of symmetries in geometry and loading, the shear component of the stress-intensity factor is zero. The normal component is found by combining the effects of the crack-face pressure σ_0 and the distributed body forces $X_1(x,y)$ and $Y_1(x,y)$ acting on layer 1. For an orthotropic material, the normal component of the stress-intensity factor may be written as follows (ref. 14):

$$k_1 = 2\sqrt{2}\frac{\mu_2^{(1)} - \mu_1^{(1)}}{\mu_2^{(1)}} \lim_{z_1^{(1)} \to a} \sqrt{z_1^{(1)} - a} \left[\phi_1' \left(z_1^{(1)} \right) + \iint_D \phi_1^{c'} \left(z_1^{(1)} \right) dx_0\, dy_0 \right] \tag{C1}$$

The function $\phi_1' \left(z_1^{(1)} \right)$, the stress potential due to the crack-face pressure σ_0, is given by the following:

$$\phi_1' \left(z_1^{(1)} \right) = \frac{\mu_2^{(1)} \sigma_0}{2\left(\mu_1^{(1)} - \mu_2^{(1)} \right)} \left(1 - \frac{z_1^{(1)}}{\sqrt{z_1^{(1)2} - a^2}} \right) \tag{C2}$$

The function $\phi_1^{c'} \left(z_1^{(1)} \right)$, the stress potential (derived in ref. 13) due to the body forces X_1 and Y_1, is given by the following:

$$\begin{aligned} \phi_1^{c'} \left(z_1^{(1)} \right) = & \frac{\mu_2^{(1)}}{\mu_1^{(1)} - \mu_2^{(1)}} \frac{1}{\sqrt{z_1^{(1)2} - a^2}} \left[A_1 F_H \left(z_1^{(1)}, w_1^{(1)}, a \right) \right. \\ & + B_1 F_H \left(z_1^{(1)}, w_2^{(1)}, a \right) + C_1 F_H \left(z_1^{(1)}, w_3^{(1)}, a \right) \\ & \left. + D_1 F_H \left(z_1^{(1)}, w_4^{(1)}, a \right) \right] + \frac{A_1}{z_1^{(1)} - w_1^{(1)}} + \frac{C_1}{z_1^{(1)} - w_3^{(1)}} \end{aligned} \tag{C3}$$

where

$$F_H(z,w,a) = \frac{\sqrt{z^2 - a^2} - \sqrt{w^2 - a^2} - (z - w)}{(z - w)}$$

and A_1, B_1, C_1, and D_1 are defined in equations (A3). Substituting equations (C2) and (C3) into (C1), taking the limit, and combining terms yield the following stress-intensity factor:

$$k_1 = \sigma_0 \sqrt{a} - \frac{2}{\sqrt{a}} \iint_D \left[T_1 \left(x, y, x_0, y_0 \right) X_1 \left(x_0, y_0 \right) + T_2 \left(x, y, x_0, y_0 \right) Y_1 \left(x_0, y_0 \right) \right] dx_0\, dy_0 \tag{C4}$$

where

$$T_1 \left(x, y, x_0, y_0 \right) = C_{11}^{(1)} \left[F_I \left(w_1^{(1)}, a \right) + F_I \left(w_3^{(1)}, a \right) \right] + C_{21}^{(1)} \left[F_I \left(w_2^{(1)}, a \right) + F_I \left(w_4^{(1)}, a \right) \right]$$

$$T_2 \left(x, y, x_0, y_0 \right) = C_{12}^{(1)} \left[F_I \left(w_1^{(1)}, a \right) + F_I \left(w_3^{(1)}, a \right) \right] + C_{22}^{(1)} \left[F_I \left(w_2^{(1)}, a \right) + F_I \left(w_4^{(1)}, a \right) \right]$$

$$F_I(w,a) = \frac{\sqrt{w^2 - a^2} - w + a}{w - a}$$

Through the use of equations (2), equation (C4) may be written in terms of the unknowns τ_x and τ_y as follows:

$$k_1 = \sigma_0 \sqrt{a} + \frac{2}{\sqrt{a}\, h_1} \iint_D \left[T_1 \left(x, y, x_0, y_0 \right) \tau_x \left(x_0, y_0 \right) + T_2 \left(x, y, x_0, y_0 \right) \tau_y \left(x_0, y_0 \right) \right] dx_0\, dy_0 \tag{C5}$$

Since the loading on layer 1 (as shown in fig. 3) is not symmetric about the y-axis, equation (C5) is valid only as z_1 approaches a, that is, at the right crack tip. To find the stress-intensity factor at the left crack tip, the function $\phi_1^{c'}\left(z_1^{(1)}\right)$ must be found for the forces X_1 and Y_1 located in the left half-plane $(z_0 = -x_0 + iy_0)$. With the new form of $\phi_1^{c'}\left(z_1^{(1)}\right)$, the same procedure as above is used to find k_1 at the left crack tip. The function $\phi_1'\left(z_1^{(1)}\right)$ does not change, since it does not depend on the location of the concentrated forces X_1 and Y_1. The stress-intensity factor at the left crack tip is thus found to be

$$k_1\big|_{x=-a} = \sigma_0\sqrt{a} - \frac{2}{\sqrt{a}\,h_1}\iint_D \left[T_3\left(x,y,x_0,y_0\right)\tau_x\left(x_0,y_0\right) + T_4\left(x,y,x_0,y_0\right)\tau_y\left(x_0,y_0\right)\right]\,dx_0\,dy_0 \tag{C6}$$

where

$$T_3\left(x,y,x_0,y_0\right) = C_{11}^{(1)}\left[F_F\left(w_1^{(1)},a\right) + F_F\left(w_3^{(1)},a\right)\right] + C_{21}^{(1)}\left[F_F\left(w_2^{(1)},a\right) + F_F\left(w_4^{(1)},a\right)\right]$$

$$T_4\left(x,y,x_0,y_0\right) = C_{12}^{(1)}\left[F_F\left(w_1^{(1)},a\right) + F_F\left(w_3^{(1)},a\right)\right] + C_{22}^{(1)}\left[F_F\left(w_2^{(1)},a\right) + F_F\left(w_4^{(1)},a\right)\right]$$

$$F_F(w,a) = \frac{\sqrt{w^2-a^2} - (w+a)}{w+a}$$

References

1. Romualdi, J. P.; Frasier, J. T.; and Irwin, G. R.: *Crack-Extension-Force Near a Riveted Stiffener.* NRL Rep. 4956, U.S. Navy, Oct. 11, 1957.
2. Sanders, J. Lyell, Jr.: *Effect of a Stringer on the Stress Concentration Due to a Crack in a Thin Sheet.* NASA TR R-13, 1959. (Supersedes NACA TN 4207.)
3. Greif, Robert; and Sanders, J. L., Jr.: The Effect of a Stringer on the Stress in a Cracked Sheet. *Trans. ASME, Ser. E: J. Appl. Mech.*, vol. 32, no. 1, Mar. 1965, pp. 59–66.
4. Bloom, J. M.; and Sanders, J. L., Jr.: The Effect of a Riveted Stringer on the Stress in a Cracked Sheet. *Trans. ASME, Ser. E: J. Appl. Mech.*, vol. 33, no. 3, Sept. 1966, pp. 561–570.
5. Poe, C. C., Jr.: *Stress-Intensity Factor for a Cracked Sheet With Riveted and Uniformly Spaced Stringers.* NASA TR R-358, 1971.
6. Poe, Clarence C., Jr.: *The Effect of Broken Stringers on the Stress Intensity Factor for a Uniformly Stiffened Sheet Containing a Crack.* NASA TM X-71947, 1974.
7. Arin, K.: A Plate With a Crack, Stiffened by a Partially Debonded Stringer. *Eng. Fract. Mech.*, vol. 6, no. 1, Mar. 1974, pp. 133–140.
8. Norris, M.: The Use of Bonded Crack-Stoppers in Pressure Cabins. *Aeronaut. J.*, vol. 85, no. 841, Feb. 1981, pp. 57–62.
9. Anderson, Jerry M.; Hsu, Teh Min; and McGee, Wade M.: Characterization of Crack Growth in Bonded Structures. *Proceedings 12th Annual Meeting of the Society of Engineering Science*, 1975, pp. 1283–1292.
10. Lekhnitskii, S. G. (S. W. Tsai and T. Cheron, transl.): *Anisotropic Plates.* Gordon & Breach Sci. Pub., Inc., c.1968.
11. Saha, Subrata: Nucleii of Strain in Two Dimensional Anisotropic Elasticity for Application to Composites. M.S. Thesis, Stanford Univ., June 1971.
12. Poe, C. C., Jr.: *A Single Fracture Toughness Parameter for Fibrous Composite Laminates.* NASA TM-81911, 1981.
13. Bigelow, Catherine Ann: The Effect of Debond Growth on Crack Propagation in Composite Plates Reinforced With Adhesively Bonded Composite Stringers. Ph.D. Thesis, Georgia Inst. of Technol., Dec. 1984.
14. Sih, G. C.; and Liebowitz, H.: *Mathematical Theories of Brittle Fracture. Fracture—An Advanced Treatise. Volume II—Mathematical Fundamentals*, H. Liebowitz, ed., Academic Press, Inc., 1968, pp. 67–190.

TABLE I. MATERIAL PROPERTIES

Material	E_x, GPa	E_y, GPa	ν_{xy}	G_{xy}, GPa	Graphite/epoxy laminate
1	51.40	51.40	0.3065	19.67	$[0/\pm 45/90]_s$
2	19.75	19.75	.7336	33.65	$[\pm 45]_{2s}$
3	129.40	10.86	.3118	5.70	[90]
4	10.86	129.40	.0262	5.70	[0]

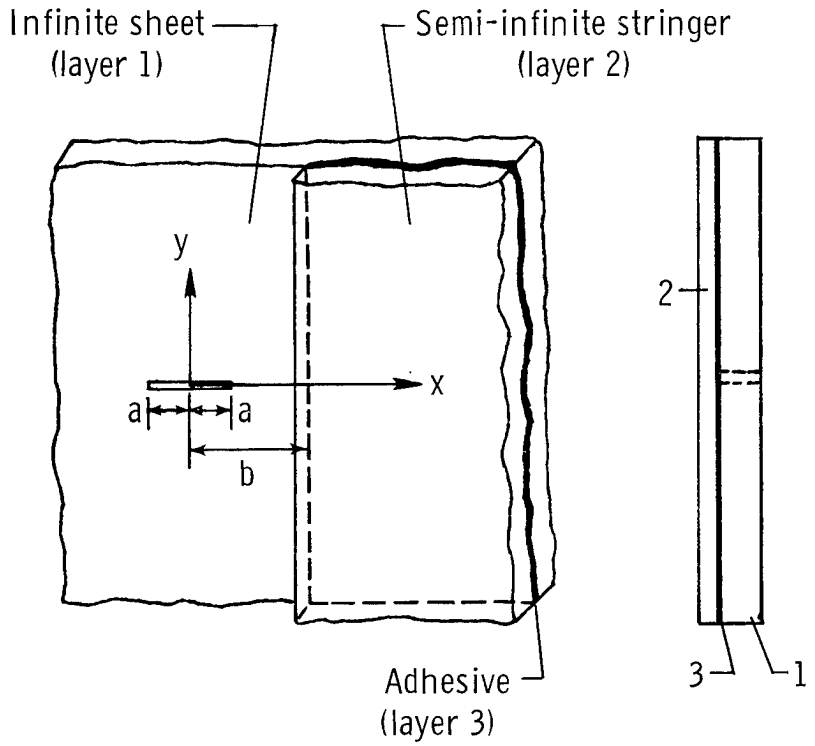

Figure 1. Sheet-stringer configuration considered in problem.

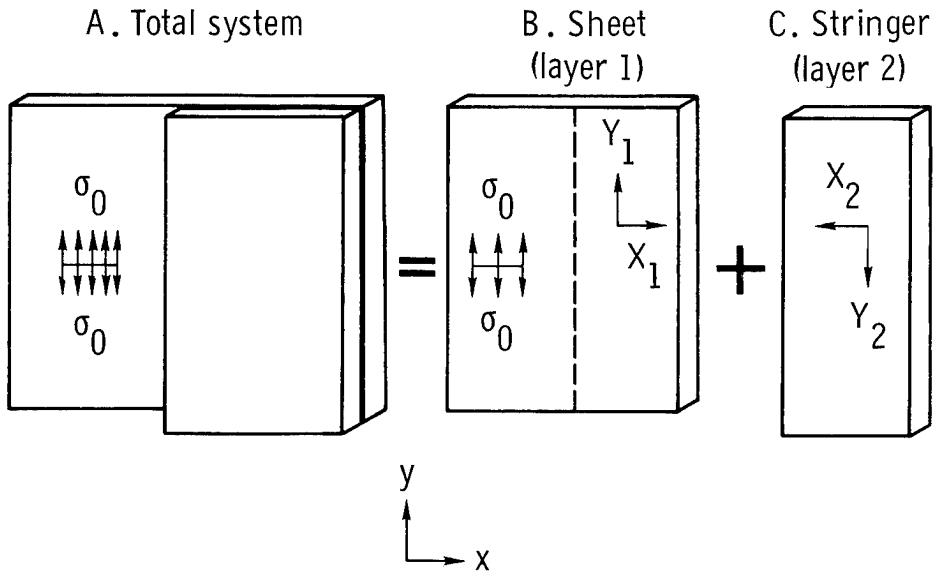

Figure 2. In-plane and interlaminar stresses for perturbation problem.

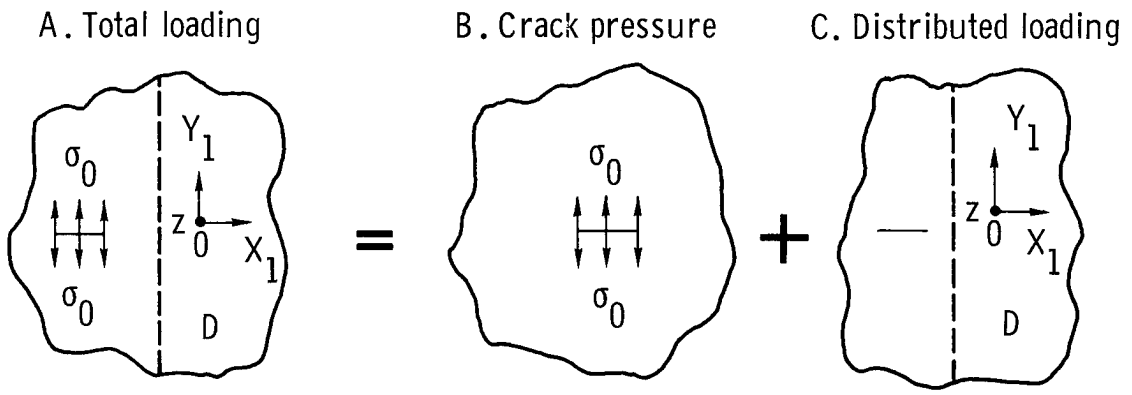

Figure 3. Superposition for sheet (layer 1).

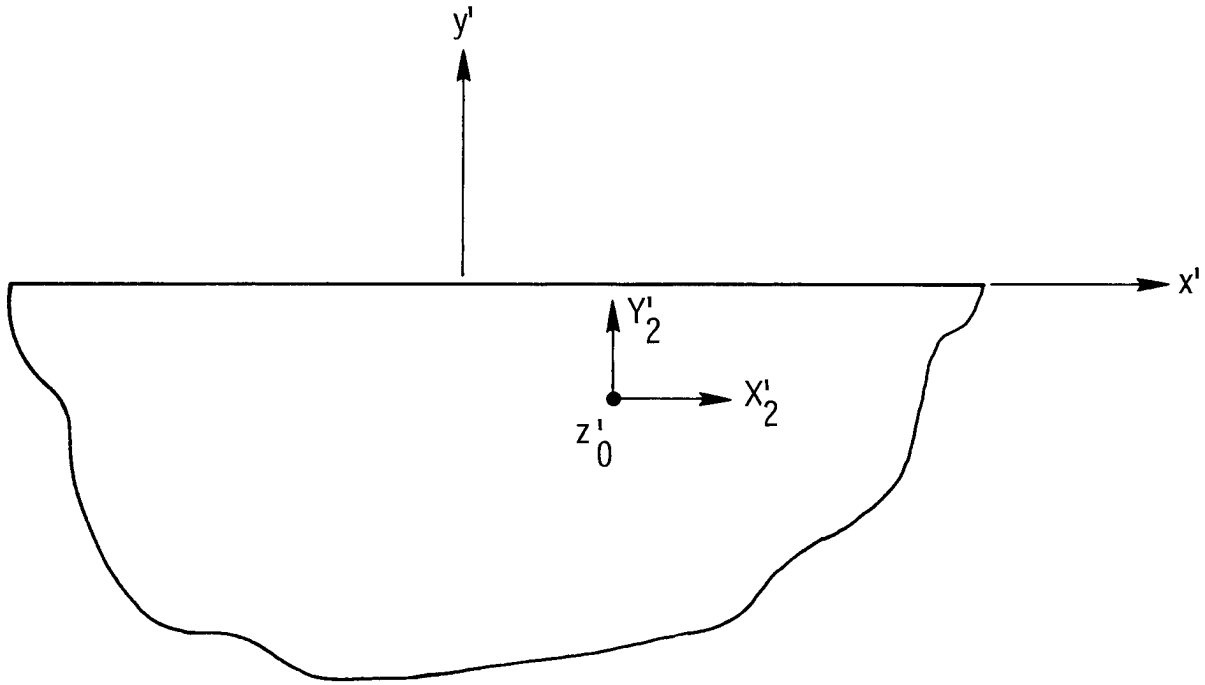

Figure 4. Loading on semi-infinite sheet (layer 2).

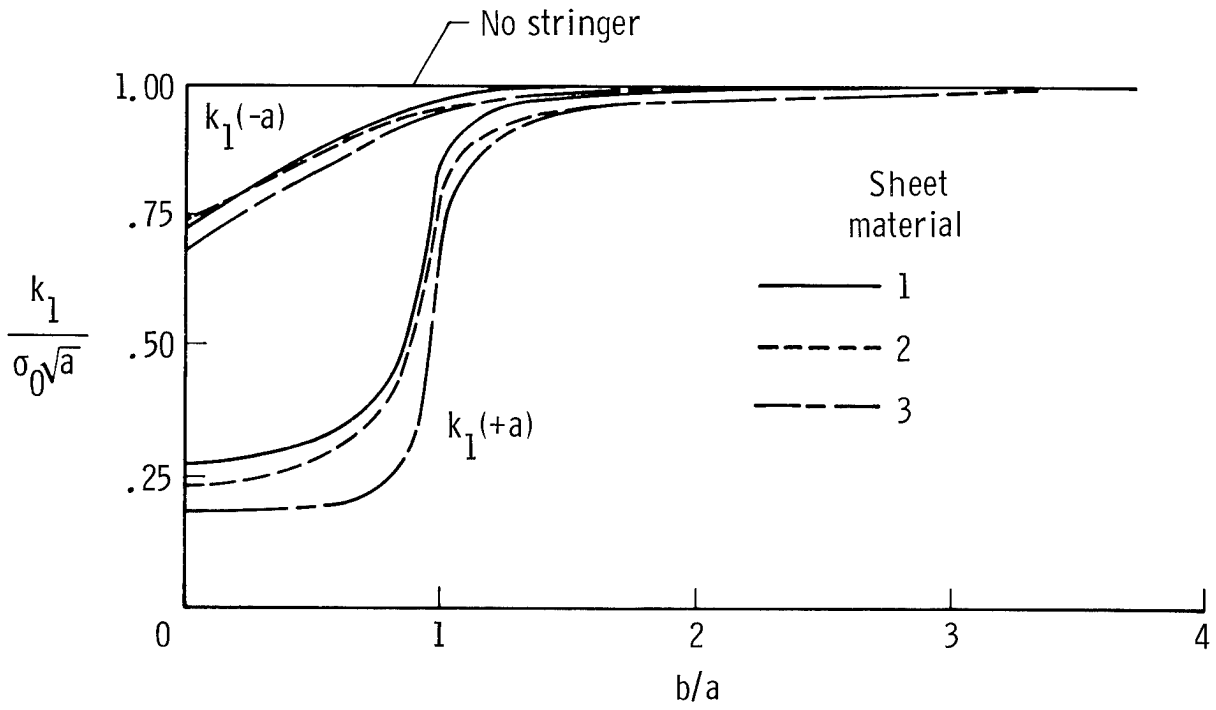

Figure 5. Normalized stress-intensity factor as function of edge distance. $a = 10$ mm; $G_3 = 460$ MPa; $h_2/h_1 = 0.5$; $h_3/h_1 = 0.005$.

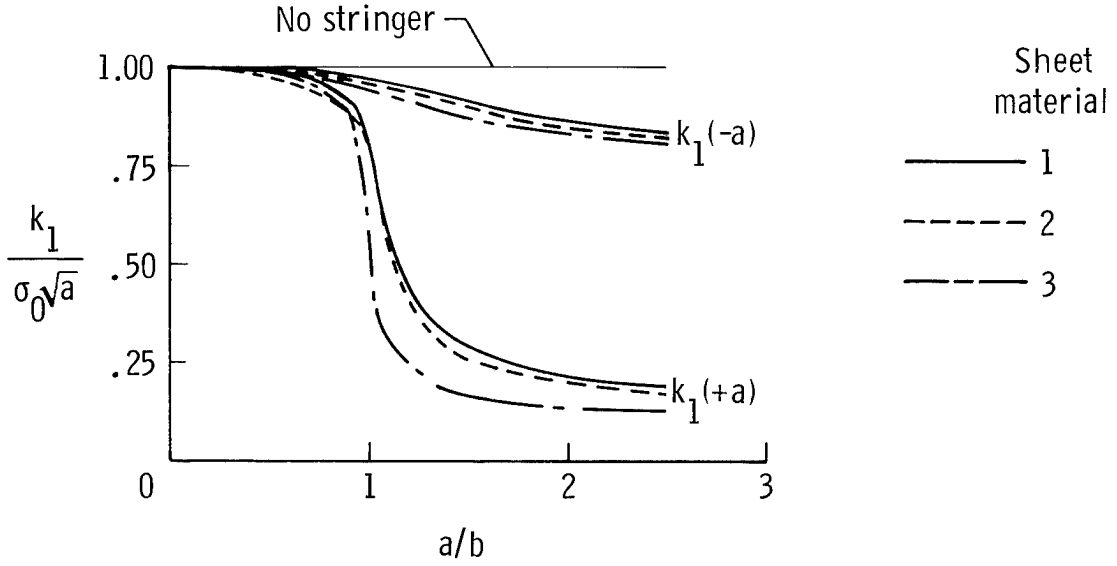

Figure 6. Normalized stress-intensity factor as function of crack length. $b = 10$ mm; $G_3 = 460$ MPa; $h_2/h_1 = 0.5$; $h_3/h_1 = 0.005$.

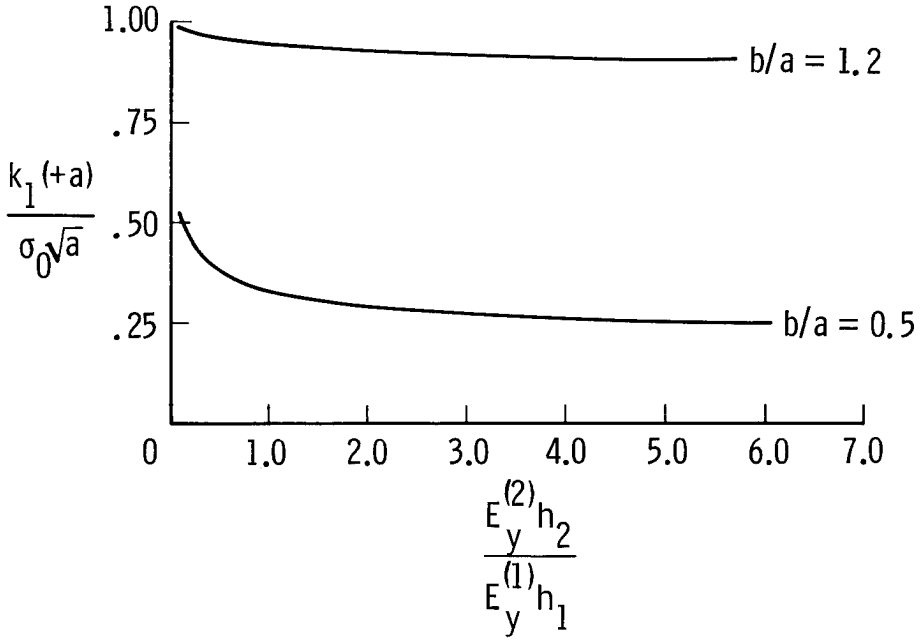

Figure 7. Normalized stress-intensity factor as function of stringer modulus.

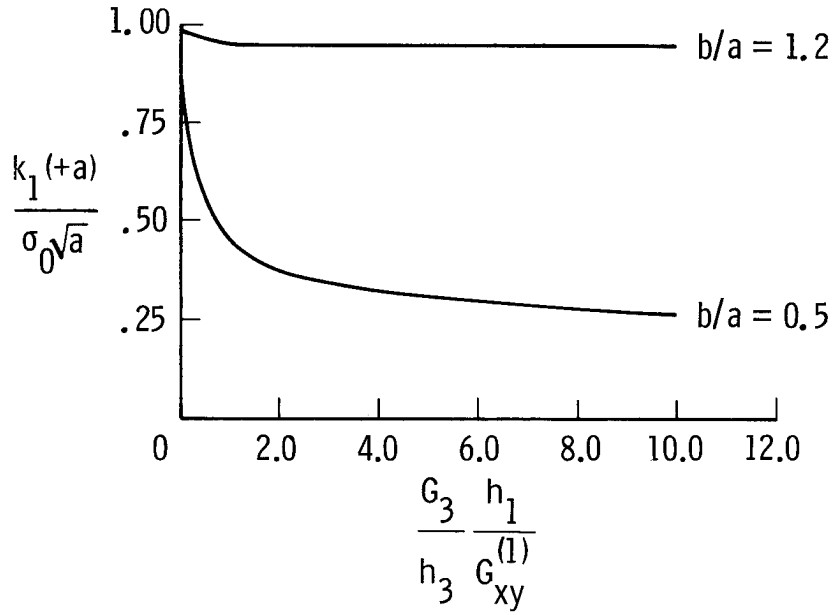

Figure 8. Normalized stress-intensity factor as function of adhesive shear modulus.

1. Report No.	2. Government Accession No.	3. Recipient's Catalog No.
NASA TP-2455		

4. Title and Subtitle	5. Report Date
A Cracked Orthotropic Sheet Stiffened by a Semi-Infinite Orthotropic Sheet	July 1985
	6. Performing Organization Code: 506-53-23-05
7. Author(s): C. A. Bigelow	8. Performing Organization Report No.: L-15972
9. Performing Organization Name and Address: NASA Langley Research Center, Hampton, VA 23665	10. Work Unit No.
	11. Contract or Grant No.
12. Sponsoring Agency Name and Address: National Aeronautics and Space Administration, Washington, DC 20546	13. Type of Report and Period Covered: Technical Paper
	14. Sponsoring Agency Code

15. Supplementary Notes

16. Abstract

The stress-intensity factor is determined for a cracked orthotropic sheet adhesively bonded to an orthotropic stringer. Since the stringer is modeled as a semi-infinite sheet, the solution is most appropriate for a crack tip located near a stringer edge. Both adherends are treated as homogeneous, orthotropic media. It is assumed they are in plane stress and the adhesive is in pure shear. From Green's functions and the complex variable theory of orthotropic elasticity developed by Lekhnitskii, a set of integral equations is obtained. The integral equations are replaced by an equivalent set of algebraic equations, which is solved to obtain the shear-stress distribution in the adhesive layer. With these stresses, equations for the stress-intensity factors at both crack tips are found. A parametric study is conducted to determine the sensitivity of the system to material properties and specimen configuration. Unless the crack tip is very close to or under the stringer, the stress-intensity factor is approximately that of an unstiffened sheet. However, as the crack propagates beneath the stringer, the stress-intensity factor decreases significantly. Increasing the stiffness of the stringer or the adhesive also results in a decrease in the stress-intensity factor.

17. Key Words (Suggested by Authors(s))
Composite materials
Stringer panel
Integral equations
Stress-intensity factors
Adhesive bond

18. Distribution Statement
Unclassified—Unlimited

Subject Category 39

19. Security Classif.(of this report)	20. Security Classif.(of this page)	21. No. of Pages	22. Price
Unclassified	Unclassified	24	A02

For sale by the National Technical Information Service, Springfield, Virginia 22161

NASA-Langley, 1985